

## Effect of Hydrothermal Alteration on Rock Properties in the Tauhara Geothermal Field, New Zealand

P. Mielke, A. Prieto, G. Bignall, I. Sass

Technische Universität Darmstadt, Geothermal Science and Technology, Schnittspahnstrasse 9, 64287 Darmstadt

mielke@geo.tu-darmstadt.de

**Keywords:** Wairakei-Tauhara, permeability, porosity, thermal conductivity, specific heat capacity, tuff, hydrothermal alteration

### ABSTRACT

Hydrothermal alteration records physicochemical changes to a rock, including dissolution and/or precipitation of new mineral phases, by its interaction with (typically) hot mineralised fluid. Transient geochemical processes can alter petro- and thermophysical rock properties. A database of hydraulic (e.g. permeability, porosity) and thermophysical parameters (e.g. thermal conductivity, heat capacity) has been established for ~450 drill cores from seven geothermal/monitor wells (TH18, THM12, THM13, THM14, THM17, THM18 and THM19) in the Tauhara Geothermal Field (Taupo Volcanic Zone (TVZ), New Zealand), including for (a) clay-altered tuff and intercalated siltstones (cap rock for the Tauhara geothermal system); (b) tuffaceous sandstones (reservoir-hosting units); and (c) rhyolitic and andesitic lavas, and their associated breccias. Hydrothermal alteration determined from XRD and shortwave infrared analysis (SWIR), optical microscopy and clay mineral characterisation, ranges from an argillic-type assemblage at shallow (< 200°C) depths to propylitic-type alteration in core from deeper and hotter (200 to >300°C) parts of the reservoir.

### 1. INTRODUCTION

This study aims to investigate the relationship between hydrothermal alteration and porosity, permeability, rock strength, thermal conductivity and associated petrophysical properties of volcanic rocks from the Tauhara geothermal field, New Zealand. Hydrothermal alteration terms the chemical alteration of a rock by hydrothermal fluids. Changing physico-chemical conditions cause a disequilibrium between the mineral assemblage of the host rock and the circulating fluids, leading to re-equilibration of the system by the formation of new mineral assemblages that are stable under the new conditions. Fluid-rock interactions of volcanic rocks with hydrothermal fluids have been investigated for decades and the geochemical mechanisms that control hydrothermal alteration are well known (Browne, 1978; Giggenbach, 1981). Hydrothermal alteration has been described in many cases and is of interest for multiple applications, be it geothermal (Browne, 1978), ore deposits (Barnes, 1997) or carbon dioxide sequestration (Matter and Kelemen, 2009) and nuclear waste storage (McCarthy et al., 1978, 1978, 1978). While the geochemical processes have been under investigation for decades and can be modeled with various software packages (e.g. PHREEQC, The Geochemist's Workbench, EQ3/EQ6, TOUGHREACT) the relation between hydrothermal alteration and the associated thermophysical rock properties have been investigated in a lesser extent. Porosity and permeability data for geothermal systems in volcanic settings were published by Bodvarsson and Witherspoon (1989) for the Wairakei and Ohaaki geothermal field in New Zealand, by Dobson et al. (2003) for the Yellowstone geothermal field in the U.S.A., and by Lenhardt and Götz (2011) for the Tepoztlán Formation in Mexico.

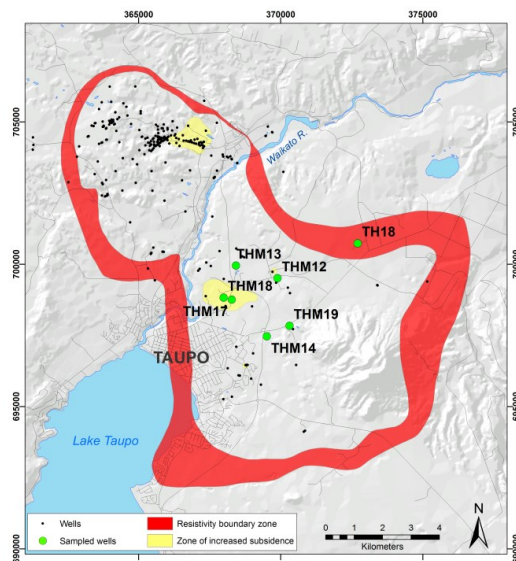


Figure 1: Map of the Wairakei-Tauhara geothermal system. Sampled wells are marked with green dots.

The Tauhara geothermal field is located in the southern part of the Taupo Volcanic Zone (TVZ), New Zealand, and is part of the larger Wairakei-Tauhara geothermal system. While the Wairakei geothermal field has been exploited for more than 50 years (Thain

and Carey, 2009), the exploitation of Tauhara has only started a decade ago. Since 2002 more than 25 deep wells were drilled at Tauhara for exploration, production and subsidence potential assessment. In 2010 the 23 MW Te Huka Power plant was commissioned by Contact Energy. The binary power plant is fed by three production wells, typically 1.1 km deep, and three injection wells with depths of 0.4 to 1.2 km. Deep wells drilled at Tauhara found evidence for a broad upflow zone beneath the field with maximum temperature recorded up to 300 °C. Resource assessment and recent numerical reservoir simulation indicate a sustainable capacity of >250 MWe (O'Sullivan and Yeh, 2010). In 2010 Contact Energy was granted resource consent for a 250 MW geothermal power station in Tauhara (a.k.a. Tauhara Phase II). The Wairakei-Tauhara geothermal system has been affected by subsidence anomalies of up to 15 m since production started half a century ago (Allis et al., 2009). Contact Energy investigated the subsidence anomalies with multiple fully cored wells drilled to depths up to 878 m inside and outside of the subsidence bowls in 2008-2009 (Rosenberg et al., 2009b). K0 consolidation tests conducted on cores obtained from these wells found anomalously high compressible rocks in volcaniclastic layers beneath the subsidence bowls, which were most likely softened by hydrothermal alteration (Bromley et al., 2010; Lynne et al., 2013). Most samples in this study derive from these wells.

## 2. CORES AND MEASUREMENT METHODS

Rock samples were selected from wells throughout the Tauhara field, with depth ranging from 289 m to 878 m. The petrology and hydrothermal alteration rank and intensity of each sample were described, and matrix permeability, porosity, density, thermal conductivity and heat capacity were measured. Samples for this study were selected from wells THM12, THM17 and THM18, which are situated inside the subsidence bowls, THM13, THM14 and THM19 from outside the subsidence anomalies, and TH18 from the boundary of the geothermal system (Figure 1). The depth intervals studied cover the Upper, Middle and Lower Huka Falls Formation, Waiora Formation and associated racetrack Rhyolite and SPA Andesite. Overlying Oruanui Formation and post Oruanui sediments have not been studied, as both formations are not of interest as productive geothermal reservoir due to their shallow depth (Rosenberg et al., 2009a). Deeper formations have not been reached by these wells.

### 2.1 Geology

Waiora Formation (WAF) and Huka Falls Formation (HFF) consist of volcaniclastic deposits and lake sediments, that were deposited in a depression in the underlying Tahorakuri Formation and Torlesse Greywacke basement. Figure 2 shows a simplified stratigraphic table and a cross section through the investigated system.

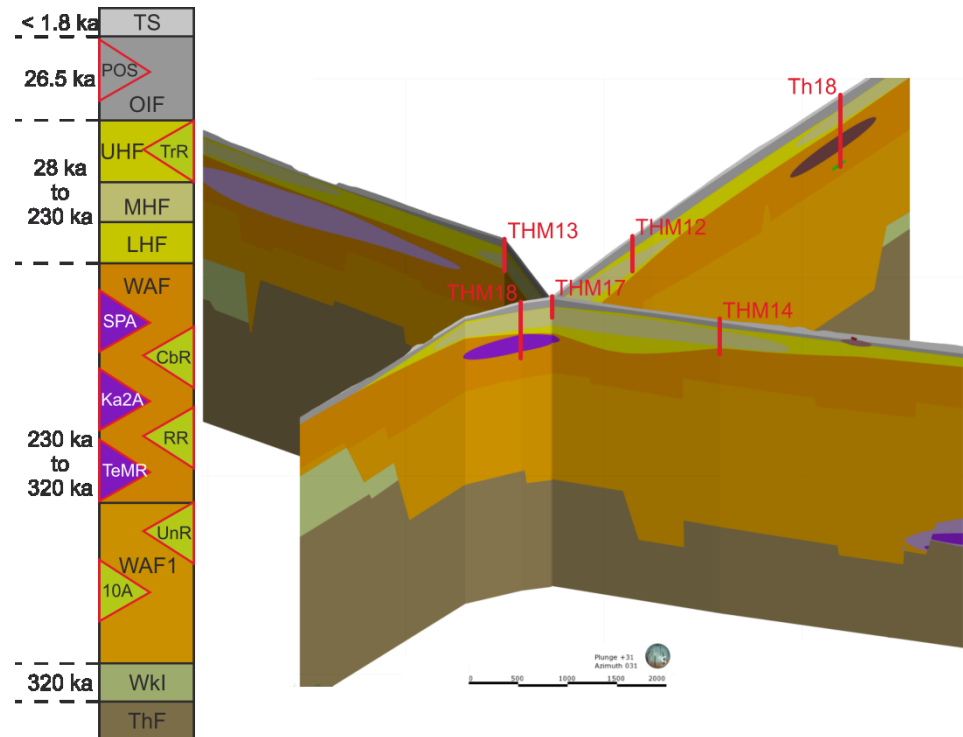


**Figure 2: Simplified stratigraphic table and cross section through some of the sampled wells. See text for stratigraphic description.**

The ca. 320 ka Waiora Formation is a 400 m to >2100 m thick and varied sequence of volcanic deposits, with interlayered mudstones, siltstones and sandstones. Various stratigraphic schemes exist to subdivide the Waiora Formation (Steiner 1977, Grindley 1965, Healy 1984), but the textural variety has made them difficult to apply. Waiora Formation host multiple intrusive andesite and rhyolite domes and associated lava breccias. It hosts the main geothermal aquifers in the Wairakei-Tauhara Geothermal System (Rosenberg et al., 2009a).

Overlying 28 ka Huka Falls Formation (HFF) is a mixture of layered sediments, breccias and tuffs, which is in contrast to the Waiora Formation dominated by sediments. HFF is subdivided into Lower, Middle and Upper units (LHF, MHF and UHF). UHF and LHF have impermeable aquiclude, while MHF has permeable tuff layers which form an important shallow aquifer. HFF acts

as an aquitards separating hot fluids in underlying permeable zones of the Waiora Formation from cool overlying groundwaters (Rosenberg et al., 2009a).

Huka Falls Formation is followed by the 26.5 old pyroclastic deposits of the Oruanui Formation (OIF). Oruanui Formation is often combined with overlying superficial deposits (post-Oruanui sediments, POS), which were formed by pyroclastic ashfall and flow units as well as soils and sediments derived from them, that are related to the Lake Taupo eruption 1.8 ka ago (Rosenberg et al., 2009a) (Rosenberg et al., 2011).

## 2.2 Measurement methods

From Aa total length of ~4 km continuous core that was available for sampling, samples were generally taken in intervals of 3 to 12 m from layers which had a thickness of at least 1 m (Rosenberg et al., 2009b), taking the lithology of the rock layers into account. Intensely brecciated and cavernous, brittle and fractured layers were not sampled, as measuring results would have been ambiguous. This led to multiple sampling gaps, e.g. in well TH18, where a ~110 m long section of brittle rocks in the UHF and MHF was not sampled, causing a shortage of samples of these formations from this well. By contrast, in homogenous layers, where one lithology is present over tens of meters, intervals were enlarged up to 22 m. This is primary the case for the andesite in well THM18 and rhyolite in TH18.

Selected core sections were about 15 cm long to allow the drilling of sample plugs with a diameter of 4 cm and a thickness of 2-3 cm. Plugs were drilled along and perpendicular to the core axis. Wells were drilled nearly vertically and layers are roughly horizontal, thus the drilled plugs can be used to measure horizontal and vertical permeability of the layers. A total of 424 samples were analyzed with 215 plugs drilled parallel to the layering and 211 perpendicular to the layering.

Sample descriptions were described using reflective light microscopy, detailing lithology and hydrothermal alteration. Short wave infrared spectroscopy (SWIR) and Methylene Blue Dye Absorption (MBT) test were conducted to determine the hydrothermal alteration mineralogy. Porosity, bulk and grain density, permeability, thermal conductivity and volumetric heat capacity were measured. Most tests were carried out on intact, oven-dry samples which have been dried for at least 24 h at 40 °C and cooled down to room temperature. Figure 3 shows the result log for well THM18.

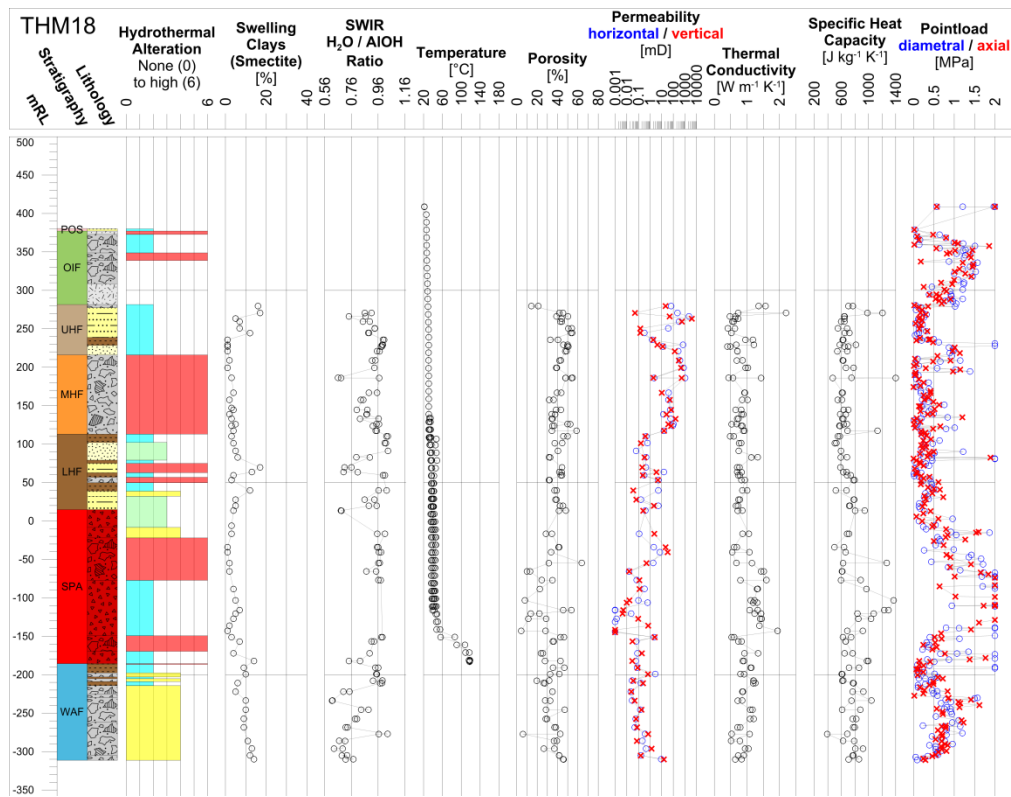


**Figure 3: Log of all conducted measurements of well THM18**

SWIR was carried out with TerraSpec 4 Hi-Res Mineral Spectrometer from ASD on oven-dried, intact samples. The device allows rapid and cost-effective qualitative clay mineral identification and, furthermore, can be used to determine illite crystallinity and general chemistry of chlorite and carbonates based on the relative intensity or wavelength position of specific absorption features (c.f. Herrmann et al., 2001; Jones et al., 2005). By calculating the H<sub>2</sub>O / AlOH ratios from both reflectance (raw) and hull quotient corrected spectra, smectite, interstratified illite-smectite and illite can be distinguished (Figure 4). In general, samples with a hull quotient corrected H<sub>2</sub>O / AlOH ratios of >0.96 correspond to illite, and <0.76 corresponds to smectite and values between 0.76 and 0.96 encompass most interstratified illite-smectite (c.f. Simpson et al., 2013).

The MBT was used to estimate the amount of swelling clays, which comprise to a large extend of smectite in this geological setting. The technique requires 1 g of oven-dry, crushed and sieved (125 micron mesh sieve) sample material. The test bases on the adsorption of Methylene Blue, an organic dye, by smectite clays and the smectite component of mixed-layer clays. The amount of smectite can be estimated on a semi-quantitative basis (c.f. Gunderson et al., 2010) by measuring the amount of adsorbed dye. The MBT is the only test which had not been carried out on intact plugs but on crushed cuttings obtained during the drilling of the plugs.

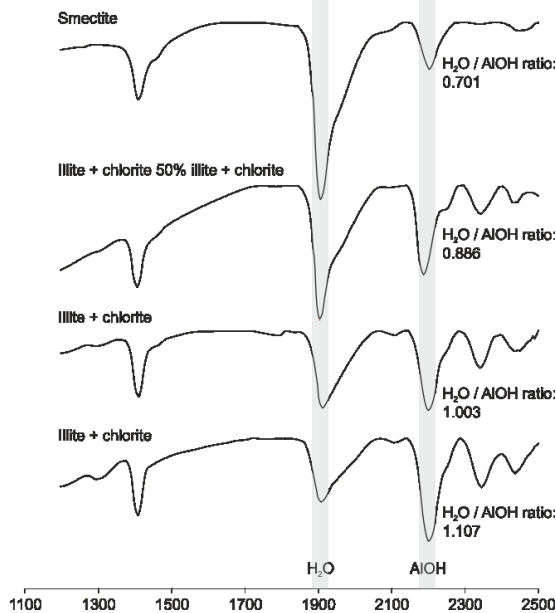


**Figure 4: Characteristic spectra for smectite, illite and some mixtures. Modified after Simpson 2013**

Porosity, bulk and grain density was measured using a gas-driven pycnometer combined with a displacement measuring technique that utilizes a fine-grained powder as quasi-fluid for the determination of the sample volume. The method allows fast but highly accurate measurements (within 0.03% accuracy and 0.02% reproducibility) of high quantities of samples. Returned values represent the gas-effective porosity.

Permeability was measured using a Hassler cell columnar permeameter, which allows permeability measurements of entire core plug samples under steady-state gas flow. Gas-driven permeability measurements have the advantage of not contaminating the sample and not affect clay-bearing samples, which may swell when tested with fluid and alter the sample (Filomena et al., 2013). The used Hassler cell is capable of measuring permeabilities ranging from 6 d to 1  $\mu$ d ( $6 \times 10^{-12} \text{ m}^2$  to  $1 \times 10^{-18} \text{ m}^2$ ).

Thermal conductivity was measured using a Lambda Measuring Center (LMC) from Geotechnical Technology Hamm & Theusner GbR. The device evaluates the thermal conductivity and thermal diffusivity by comparison with known standards. The relation between standard and sample is:

$$\lambda_{\text{sample}} = \lambda_{\text{standard}} \frac{\Delta T_{\text{standard}}}{\Delta T_{\text{sample}}}$$

where  $\lambda$  and  $\Delta T$  are thermal conductivity and temperature difference respectively. The measuring process  $\lambda$  is divided in four parts. First, the instrument determines the temperature drift at the surface of the sample to ensure steady temperature conditions. A temperature sensor measures the initial temperature of the specimen. Subsequently, a 150 Watt infrared emitter heats up the specimen for two seconds. The surface temperature of the specimen is logged during the heating and following cooling time and  $\Delta T$  is calculated in the third second of the analyzing process.

To determine the thermal diffusivity  $\kappa$  the sample is heated a second time, but the temperature is logged in a distance  $x$  from the heated spot. After time  $\tau$  the heating process leads to a temperature maximum at the detecting point. The thermal diffusivity is then calculated by:

$$\tau = \frac{x^2}{6\kappa}$$

Thermal diffusivity of the sample is also determined by comparison with the standard:

$$\kappa_{\text{sample}} = \kappa_{\text{standard}} \frac{\Delta \tau_{\text{standard}}}{\Delta \tau_{\text{sample}}}$$

By including the bulk density combined with  $\lambda$  and  $\kappa$ , the specific heat capacity  $c_p$  is calculated:

$$c_p = \frac{\lambda}{\tau \cdot \rho_b}$$

### 2.3 Lithology and hydrothermal alteration

The studied core sections of all wells primary consist of volcanic deposits (tuff and volcanic breccias), lake sediments (sandstone, siltstone and mudstone) and intrusive andesite and rhyolite lavas and their associated breccias. For this study samples have been classified into the volcaniclastic deposits, i.e. tuff and volcanic breccia; sedimentary deposits, i.e. sandstone, siltstone and mudstone; and lavas and their associated breccias, i.e. andesite lava, andesite breccia, rhyolite lava and rhyolite breccia.

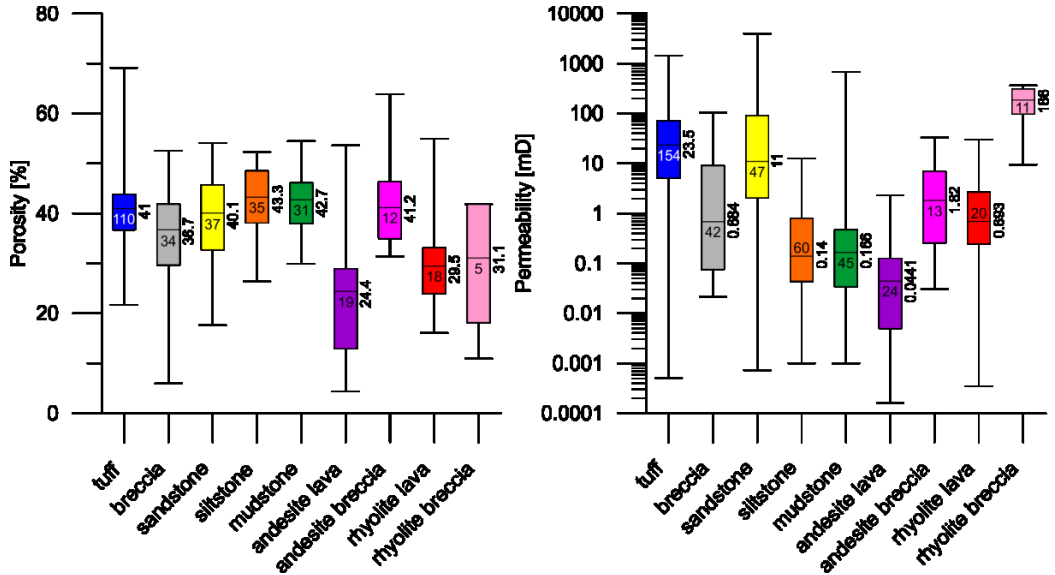


**Figure 5: Porosity and permeability of all sample classes. Sample numbers per class are shown in the boxes, the median is shown right to each box.**

Hydrothermal alteration typically follows a prograde trend with depth. Shallow formations, which are usually cooler than 230 °C are affected by argillic alteration and primary comprise smectite, illite and smectite-illite mixed-layer clays. Deeper, hotter (200 °C – 300 °C) zones are commonly affected by propylitic alteration and comprise chlorite, quartz and epidote and accessory albite, adularia, carbonates, pyrite, zeolites such as wairakite, prehnite and titanite.

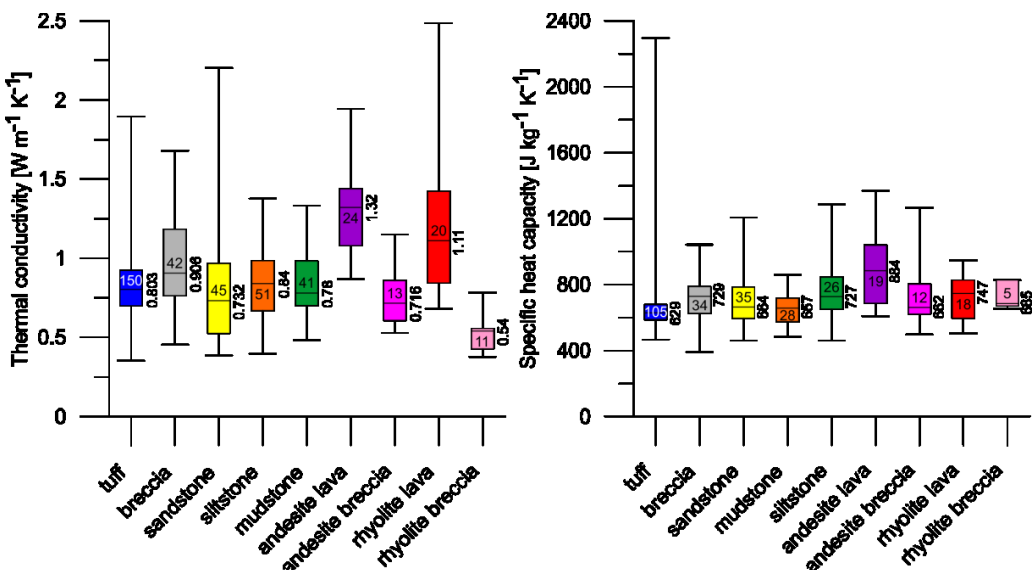


**Figure 6: Thermal conductivity and specific heat capacity of all sample classes. Sample numbers per class are shown in the boxes, the median is shown right to each box.**

Tuffs and volcaniclastic breccias are commonly poorly sorted pumice-rich and crystal-rich. Phenocrysts are quartz and common plagioclase in a microcrystalline and vitroclastic groundmass of plagioclase and quartz. Lithics include andesites and rhyolites as

well as sandstone and mudstones fragments. Tuffs and breccias are massive and have no apparent bedding. Hydrothermal alteration ranges from weak to intense and increases with depth. Minerals include smectite, smectite-illite mixed-layer clays, chlorite, hydrothermal quartz, pyrite, leucoxenes (anatase) and rare kaolinite. Plagioclase is slightly altered in shallow depths, and replaced by calcite, adularia, chlorite/clay, zeolites (mordenite) and rare wairakite in deeper zones. Iron-magnesium minerals (e.g. pyroxenes) are commonly completely replaced by clay and chlorite. Pumice clasts and glassy matrix are often selectively altered to clay.

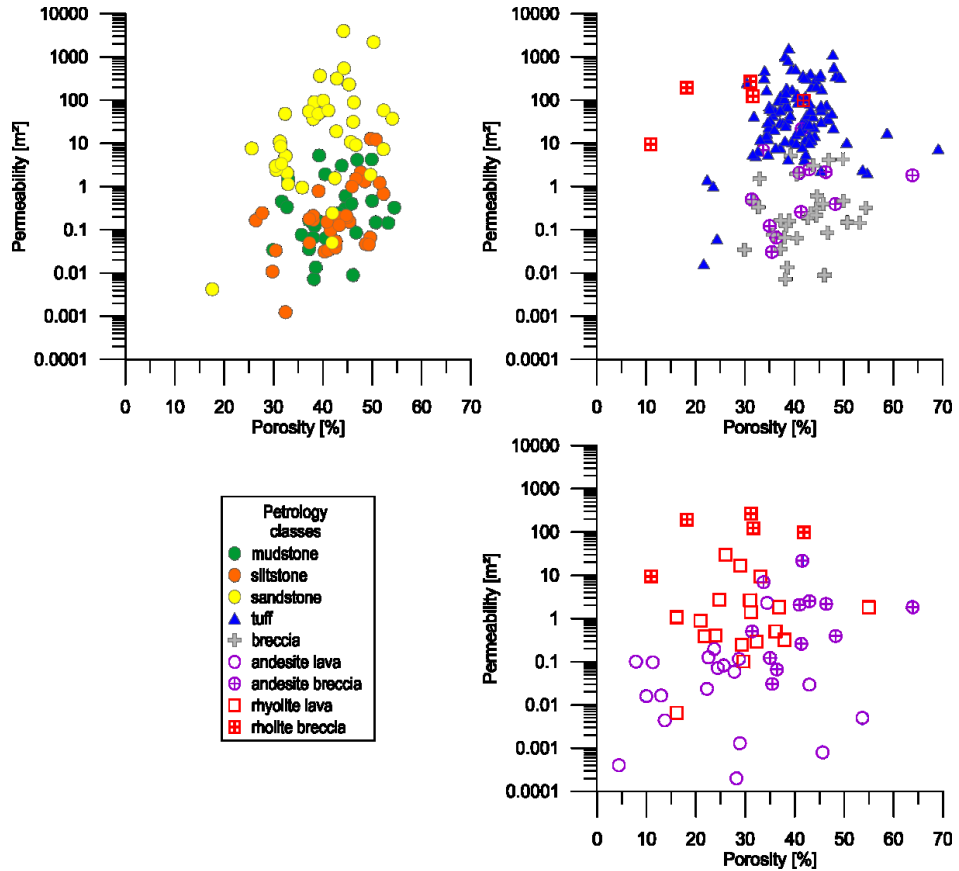


**Figure 7: Cross plot of porosity and permeability for all samples classified by lithology**

Sandstones are commonly planar-bedded or gently inclined, well sorted and very fine to fine-grained to rarely coarse-grained. Grains consist of quartz and plagioclase, with minor clasts of rhyolite, andesite and pumice. Hydrothermal alteration of sandstones is commonly moderate to intensive with abundant chlorite, clay (smectite-illite mixture), rare fine-grained granular secondary quartz and pyrite. Intense hydrothermal alteration almost completely obliterates the primary minerals and masks the primary texture. Siltstones and mudstones are commonly massive or show fine lamination. Hydrothermal alteration is generally weak to moderate and exhibits a mineral assemblage of common calcite, quartz, rare pyrite and clay (commonly smectite-illite mixed-layer clays, minor smectite, rare kaolinite and rare chlorite). Chlorite alteration is bedding-restricted.

Rhyolite units comprise of rhyolite lava and rhyolite breccia. The rhyolite lava is massive, almost aphyric or porphyritic (usually less than 1% phenocrysts of plagioclase and quartz) lava body. The texture is glassy (obsidian) and exhibits flow banding. The monomict rhyolite breccias contain subrounded to subangular clasts of lapilli or blocky size with minor quartz or feldspar crystals. The clasts are flow banded rhyolite in a fine-grained glassy matrix. Hydrothermal alteration is generally weak in the upper parts and increases with depth to high intensity. Alteration is to common clay (smectite) and minor to common pyrite (chalcopyrite). Hydrothermal quartz, clay (illite) and pyrite overprints most of the primary textures of the rock in the moderately to highly altered rhyolites. Many rhyolites are very strong due to intense silicification.

Andesites are subdivided in andesite lava and andesite breccia. The lava has a characteristic trachytic texture with minor flow banding and consists of plagioclase (~90%), rare clinopyroxenes (~5%) and minor quartz. The microlithic groundmass consists of plagioclase and rare iron-oxides. Crystals are euhedral to subhedral and up to 1 cm in length. The andesite lava is relatively fresh with unaltered pyroxenes, minor clay (smectite-illite) or calcite can occur. The andesite breccia consists of andesite fragments comprising of plagioclase phenocrysts (>95%) in a trachytic matrix of glass and plagioclase. Plagioclase phenocrysts are euhedral or subhedral and up to 1 cm long. The breccia is cemented with chalcedony and quartz and has accessory zeolites such as mordenite. It is moderately to highly altered to chlorite, quartz and clay. Andesitic clasts are silicified.

### 3 Thermophysical rock properties and alteration

Figure 5 shows the porosity and permeability ranges for all sample classes. Porosity commonly has a range of ~20%, rarely up to 50%, however, the interquartile range spans commonly spans ~10% to 15%, rarely more. Permeability often spans up to 6 magnitudes, while the interquartile range is commonly limited to one or two magnitudes. Tuffs commonly have a porosity range of

36% to 44% and permeability ranging from 5 mD to 71 mD. Breccias have the lowest porosity (29% to 42%) of all sedimentary and volcaniclastic samples, and common permeability of 0.07 mD to 9 mD, which is close to those of siltstones and mudstones. Sandstones commonly have porosity (32% to 46%) and permeability (2 mD to 90 mD) similar to those of tuffs. Siltstones and mudstones have the highest porosities of all samples (siltstone: 38% to 48%, mudstone: 38% to 46%), but also the lowest permeability (siltstone: 0.04 mD to 0.8 mD, mudstone: 0.03 to 0.5 mD), except for the andesite lava. Permeability of sedimentary and volcaniclastic rocks generally increases with grain size, while porosity decreases. Andesite and rhyolite lavas commonly have low porosities (andesite: 13% to 29%, rhyolite 23% to 33%) but permeability differs in more than one order. The permeability of andesite ranges from 0.005 mD to 0.1 mD, while rhyolite has 0.25 mD to 2.6 mD. Andesite breccias have porosities of 35% to 46%, while rhyolite breccias range from 18% to 42%. Permeability of both lava breccias differs significantly, with andesite breccias ranging from 0.2 mD to 6.9 mD, while rhyolite breccias range from 98 mD to 306 mD.

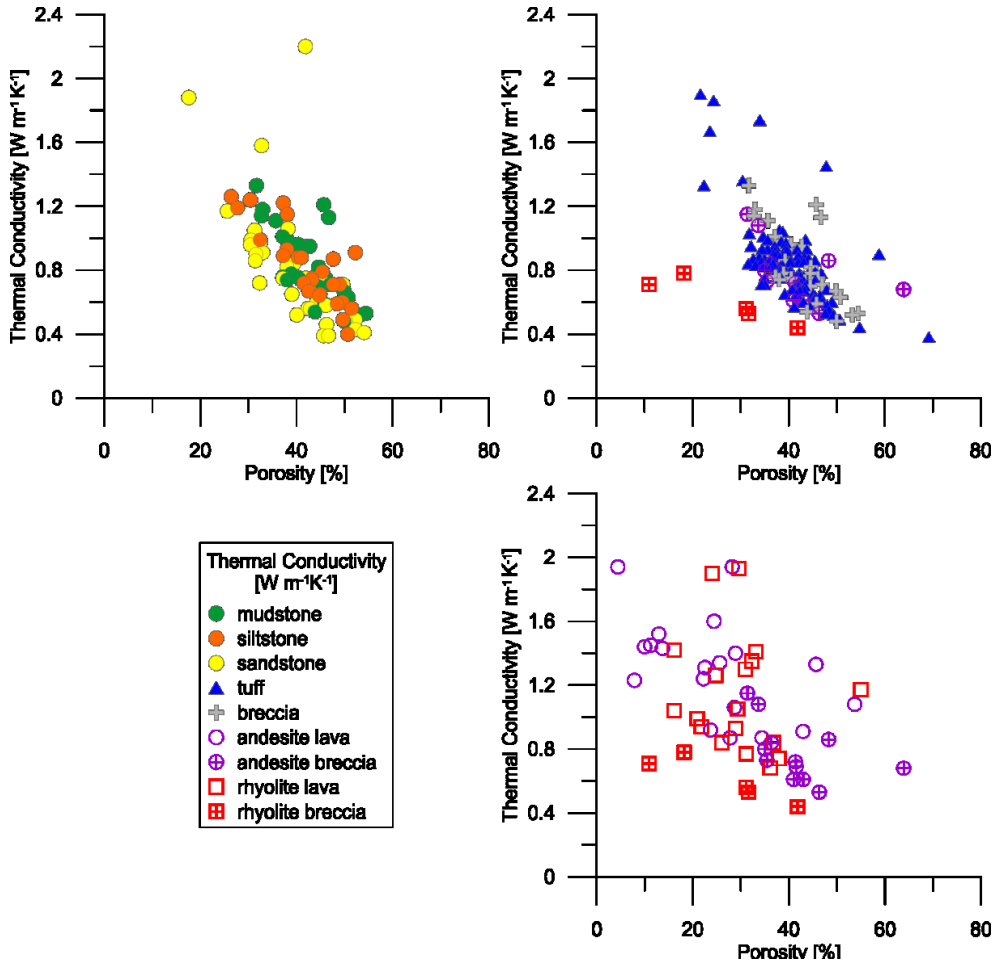


**Figure 8: Cross plot of porosity vs. thermal conductivity for all sample grouped by lithology classes**

Thermal conductivity and specific heat capacity ranges for all sample classes are shown in Figure 6. Similar to the porosity and permeability the range is often far bigger than the interquartile range, which commonly has a spanning range of  $0.5 \text{ W m}^{-1}\text{K}^{-1}$  to  $1 \text{ W m}^{-1}\text{K}^{-1}$  and  $\sim 200 \text{ J kg}^{-1}\text{K}^{-1}$ , respectively. Thermal conductivity typically increases with porosity and is independent from permeability. Sedimentary samples, breccias and tuff samples have thermal conductivities below  $1 \text{ W m}^{-1}\text{K}^{-1}$ , while the lavas have thermal conductivities up to  $1.5 \text{ W m}^{-1}\text{K}^{-1}$ . The rhyolite breccia has the lowest thermal conductivity of all samples ( $< 0.5 \text{ W m}^{-1}\text{K}^{-1}$ ). The specific heat capacity shows minor deviations, most samples except the andesite lava are in the same range of  $\sim 580 \text{ J kg}^{-1}\text{K}^{-1}$  to  $\sim 800 \text{ J kg}^{-1}\text{K}^{-1}$ .

When permeability (Figure 7) and thermal conductivity (Figure 8) results are plotted versus porosity and classified by lithology, most samples, especially the sediments and volcanicastics, plot within denser point clusters. Clusters often overlap, but trends are visible. Siltstones and mudstones plot with the same cluster for both permeability-porosity and thermal conductivity-porosity, which points to a high lithological similarity. Both classes could be merged to one class. Tuffs and breccias, which technically only differ in their amount and size of lithics, plot in different permeability-porosity clusters but share a cluster in the thermal conductivity-porosity plot. The andesite breccias are similar to the volcaniclastic breccias, while the rhyolite breccia differs.

Figure 9 (left) shows plots of direction-dependent data for all lithology classes. Sedimentary samples, especially sandstones, have a higher horizontal permeability, which could be related to fine bedding structures. Tuffs show no direction-dependency. Lavas and their breccias show no trend, however, the sample number is too for a qualified analysis.

Data from axial and diametral pointload were taken from tests described in Bromley et al. (2010). These tests were conducted on all wells from the Tauhara Subsidence Project in intervals of few meters. The sampling depths for the pointload strength tests were matched with the sample depths for the plugs for this study. The data reveals a slightly higher axial strength for most samples (Figure 9, right). Rock strength of tuff commonly decreases with increasing alteration, and increases with depth (Figure 10). Weakly altered tuffs have the highest permeability ( $>100$  mD), while moderately altered samples have lower permeabilities (10 mD to 100 mD). Highly altered tuffs have the full range of permeability (Figure 11, left). Porosity decreases with alteration intensity, but the effect is only vague. Furthermore, tuffs with a low amount of smectite (<4%) commonly have one magnitude higher permeabilities than samples with higher amounts of smectite. By contrast, the type of clay (i.e. smectite, illite-smectite and/or illite) has no impact on permeability (Figure 12). Thermal conductivity of tuff increases with hydrothermal alteration intensity. Weakly to moderately altered tuffs have permeabilities in the range of  $0.4 \text{ W m}^{-1}\text{K}^{-1}$  to  $0.9 \text{ W m}^{-1}\text{K}^{-1}$ , highly altered tuffs have thermal conductivities  $>0.7 \text{ W m}^{-1}\text{K}^{-1}$  (Figure 11, right).

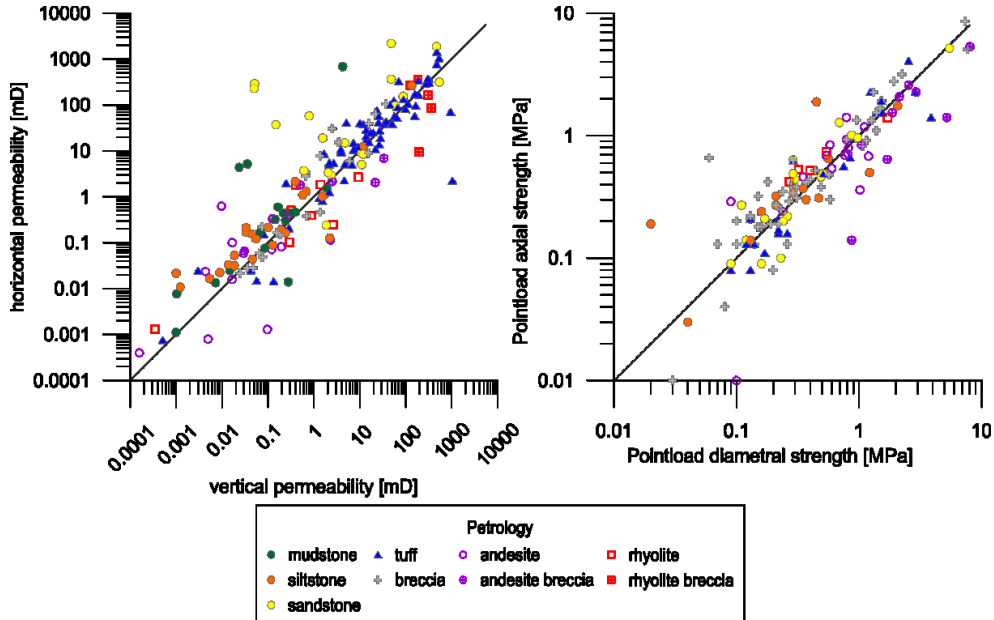


Figure 9: Cross plot of horizontal and vertical permeability and axial and diametral pointload strength for all lithology classes. Horizontal permeability is  $\sim 50\%$  higher than vertical permeability for sedimentary classes.

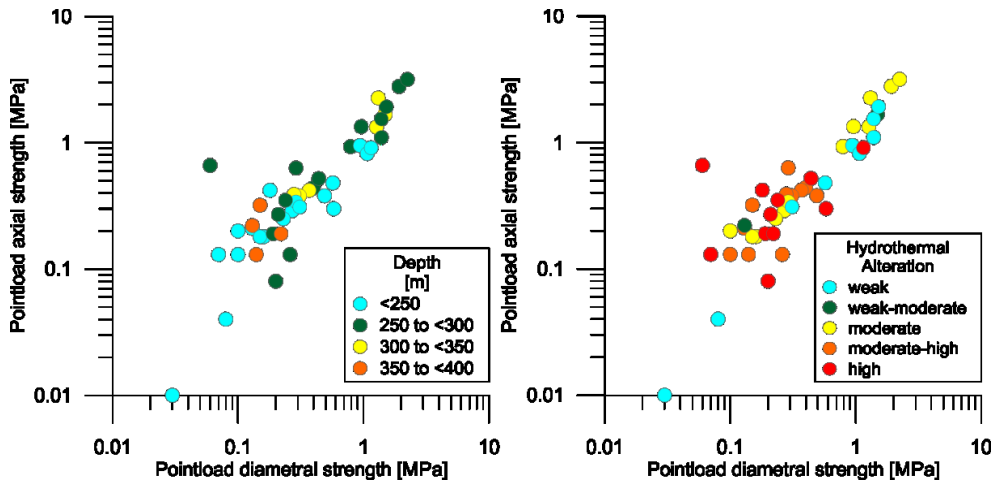


Figure 10: Cross plot of depth (left) and alteration (right) with pointload strength of tuff samples

#### 4 CONCLUSION

The thermophysical rock properties 424 rock samples from nine lithology classes (tuff, breccia, sandstone, siltstone, mudstone, andesite lava and breccia, rhyolite lava and breccia) have been measured and the correlation with hydrothermal alteration intensity has been investigated. Variations in permeability, porosity, thermal conductivity and specific heat capacity are related to lithology and intensity and nature of hydrothermal alteration. Porosity of the volcaniclastic and sedimentary rocks is in the same range, while the permeability is significantly different among them. Tuffs and sandstones have the highest permeability, and siltstones, mudstones and breccias have up to three orders of magnitudes lower permeability. Lava breccias commonly have two magnitudes higher permeability than the associated lava, although their porosity differs in a far smaller extend. Thermal conductivity is closely related to porosity, which in turn seems to decrease with increasing hydrothermal alteration.

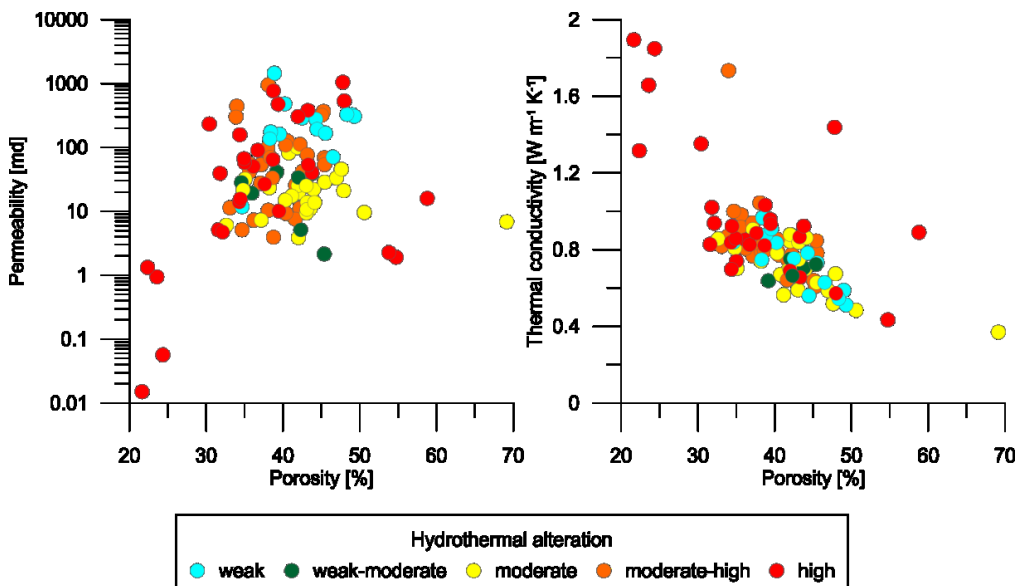


Figure 11: Impact of hydrothermal alteration porosity and permeability (left) and thermal conductivity (right)

Porosity and permeability of tuffs are in the same range as values reported from other geothermal systems. Bodvarsson and Witherspoon (1989) reported permeability values of 30-40 mD, and porosities of 20% for the Wairakei and Ohaaki geothermal fields. Dobson et al. (2003) reported porosities of 3 to 57%, and permeabilities of 0.002 up to 5000 mD, depending on lithology, for the Yellowstone geothermal system. Lenhardt and Götz (2011) studied volcanic deposits and lavas of the Tepoztlán Formation and reported porosity and permeability values of 1.4% to 56.7% and 1.2 mD to 594.6 mD, respectively.

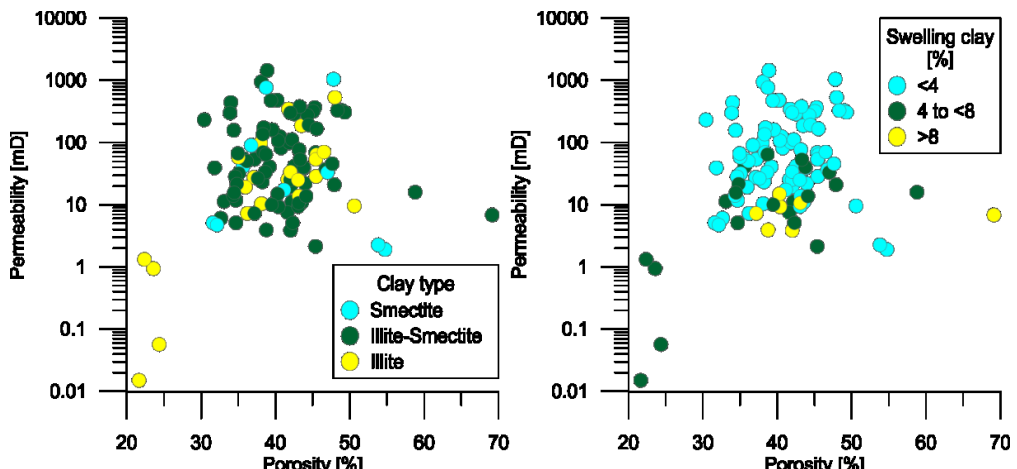


Figure 12: Cross plots of permeability and porosity with respect to clay type (left) and amount of swelling clays (right)

## REFERENCES

Allis, R., Bromley, C., Currie, S., 2009. Update on subsidence at the Wairakei–Tauhara geothermal system, New Zealand. *Geothermics* 38 (1), 169–180.

Barnes, H.L., 1997. *Geochemistry of hydrothermal ore deposits*, 3rd ed. ed. Wiley, New York, xx, 972.

Bodvarsson, G., Witherspoon, P., 1989. *Geothermal Reservoir Engineering*. Geothermal science and technology (2).

Bromley, C.J., Currie, S., Ramsay, G., Rosenberg, M.D., Pender, M., O'Sullivan, M., Lynne, B., Lee, S.-G., Brockbank, K., Glynn-Morris, T., Mannington, W., Garvey, J., 2010. Tauhara Stage II Geothermal Project : subsidence report: GNS Science consultancy report 2010/151.

Browne, P., 1978. Hydrothermal Alteration in Active Geothermal Fields. *Annu. Rev. Earth Planet. Sci.* 6 (1), 229–248.

Dobson, P.F., Kneafsey, T.J., Hulen, J., Simmons, A., 2003. Porosity, permeability, and fluid flow in the Yellowstone geothermal system, Wyoming. *Journal of Volcanology and Geothermal Research* 123 (3-4), 313–324.

Filomena, C.M., Hornung, J., Stollhofen, H., 2013. Assessing accuracy of gas-driven permeability measurements: a comparative study of diverse Hassler-cell and probe permeameter devices. *Solid Earth Discuss.* 5 (2), 1163–1190.

Giggenbach, W.F., 1981. Geothermal mineral equilibria. *Geochimica et Cosmochimica Acta* 45 (3), 393–410.

Gunderson, R., Cumming, W., Astra, D., Harvey, C., 2010. Analysis of smectite clays in geothermal drill cuttings by the methylene blue method: for well site geothermometry and resistivity sounding correlation, in: Proceedings World Geothermal Congress 2010. World Geothermal Congress 2010, Bali, Indonesia. 25-30 April 2010.

Herrmann, W., Blake, M., Doyle, M., Huston, D., Kamprad, J., Merry, N., Pontual, S., 2001. Short Wavelength Infrared (SWIR) Spectral Analysis of Hydrothermal Alteration Zones Associated with Base Metal Sulfide Deposits at Rosebery and Western Tharsis, Tasmania, and Highway-Reward, Queensland. *Economic Geology* 96 (5), 939–955.

Jones, S., Herrmann, W., Gemmell, J.B., 2005. Short Wavelength Infrared Spectral Characteristics of the HW Horizon: Implications for Exploration in the Myra Falls Volcanic-Hosted Massive Sulfide Camp, Vancouver Island, British Columbia, Canada. *Economic Geology* 100 (2), 273–294.

Lenhardt, N., Götz, A.E., 2011. Volcanic settings and their reservoir potential: An outcrop analog study on the Miocene Tepoztlán Formation, Central Mexico. *Journal of Volcanology and Geothermal Research* 204 (1-4), 66–75.

Lynne, B.Y., Pender, M., Glynn-Morris, T., Sepulveda, F., 2013. Combining scanning electron microscopy and compressibility measurement to understand subsurface processes leading to subsidence at Tauhara Geothermal Field, New Zealand. *Engineering Geology* 166, 26–38.

Matter, J.M., Kelemen, P.B., 2009. Permanent storage of carbon dioxide in geological reservoirs by mineral carbonation. *Nature Geosci* 2 (12), 837–841.

McCarthy, G.J., White, W.B., Roy, R., Scheetz, B.E., Komarneni, S., Smith, D.K., Roy, D.M., 1978. Interactions between nuclear waste and surrounding rock. *Nature* 273 (5659), 216–217.

O'Sullivan, M., Yeh, A., 2010. Wairakei-Tauhara Modelling Report.

Rosenberg, M.D., Bignall, G., Rae, A.J., 2009a. The geological framework of the Wairakei–Tauhara Geothermal System, New Zealand. *Geothermics* 38 (1), 72–84.

Rosenberg, M.D., Ramirez, L.E., Kilgour, G.N., Milicich, S.D., Manville, V.R., 2009b. Tauhara Subsidence Investigation Project: geological summary of Tauhara wells THM12-18 and THM21-22, and Wairakei wells WKM14-15: GNS Science consultancy report 2009/309.

Simpson, M., Rae, A., Ganefianto, N., Sepulveda, F., 2013. Short wavelength infrared (SWIR) spectral characterisation of smectite, illite-smectite and illite for geothermal fields of the Taupo Volcanic Zone, New Zealand, in: 35th New Zealand Geothermal Workshop proceedings. 35th New Zealand Geothermal Workshop, Rotorua, New Zealand. 17-20 November 2013.

Thain, I.A., Carey, B., 2009. Fifty years of geothermal power generation at Wairakei. *Geothermics* 38 (1), 48–63.